Research Square

Preprints are preliminary reports that have not undergone peer review.
They should not be considered conclusive, used to inform clinical practice,
or referenced by the media as validated information.

KMT9 drives epithelial-mesenchymal plasticity and invasion in prostate cancer

Eric Metzger

eric.metzger@uniklinik-freiburg.de

Uniklinikum Freiburg https://orcid.org/0000-0002-1394-1083

Jon Peñarando

Ling Peng

Klinik für Urologie und Zentrale Klinische Forschung, Klinikum der Albert-Ludwigs-Universität Freiburg, Freiburg, Germany

Sheng Wang

Klinik für Urologie und Zentrale Klinische Forschung, Klinikum der Albert-Ludwigs-Universität Freiburg, Freiburg, Germany

Dominica Willmann

Uniklinikum Freiburg

Franziska Pfefferle

Klinik für Urologie und Zentrale Klinische Forschung, Klinikum der Albert-Ludwigs-Universität Freiburg, Freiburg, Germany

Astrid Rieder

Klinik für Urologie und Zentrale Klinische Forschung, Klinikum der Albert-Ludwigs-Universität Freiburg, Freiburg, Germany

Manuela Sum

Klinik für Urologie und Zentrale Klinische Forschung, Klinikum der Albert-Ludwigs-Universität Freiburg, Freiburg, Germany

Sylvia Urban

Klinik für Urologie und Zentrale Klinische Forschung, Klinikum der Albert-Ludwigs-Universität Freiburg, Freiburg, Germany

Daniel Metzger

IGBMC Strasbourg https://orcid.org/0000-0002-5555-046X

Manfred Jung

Albert-Ludwigs-Universität Freiburg https://orcid.org/0000-0002-6361-7716

Christian Gratzke

Roland Schüle

Uniklinikum Freiburg https://orcid.org/0000-0001-8147-634X

Article

Keywords: Histone methyltransferase, KMT9, EMT, invasion, prostate cancer

Posted Date: November 20th, 2026

DOI: https://doi.org/10.21203/rs.3.rs-11649851/v1

License: This work is licensed under a Creative Commons Attribution 4.0 International License.
Read Full License

Additional Declarations:
There is **NO** conflict of interest to disclose.

Table 1 is available in the Supplementary Files section.

KMT9 drives epithelial-mesenchymal plasticity and invasion in prostate cancer

Jon Peñarando[1,4,#], Ling Peng[1], Sheng Wang[1], Dominica Willmann[1], Franziska Pfefferle[1], Astrid Rieder[1], Manuela Sum[1], Sylvia Urban[1], Christian Gratzke[1], Daniel Metzger[2], Manfred Jung[3], Roland Schüle[1,2], Eric Metzger[1,4,#]

[1]Klinik für Urologie und Zentrale Klinische Forschung, Klinikum der Albert-Ludwigs-Universität Freiburg, Freiburg, Germany.

[2]Institut de Génétique et de Biologie Moléculaire et Cellulaire, CNRS UMR7104, INSERM U964, Université de Strasbourg, Illkirch, France.

[3]Institute of Pharmaceutical Sciences, Albert-Ludwigs-Universität Freiburg, Freiburg, Germany.

[4]German Cancer Consortium (DKTK), Partner site Freiburg, a partnership between DKFZ and Medical Center - University of Freiburg.

[#]Correspondence and requests for materials should be addressed to E.M. (eric.metzger@uniklinik-freiburg.de) and J.P. (Jon.penarando.saez@uniklinik-freiburg.de)

Abstract

Epithelial-mesenchymal transition (EMT) is a dynamic and reversible cell-state transition program that triggers tumour cell plasticity contributing to increase tumour heterogeneity, invasiveness and metastasis. Despite advances in the field, pharmacological strategies to target tumour plasticity remain limited. Here, we identify the histone lysine methyltransferase KMT9 as a novel epigenetic regulator of epithelial-mesenchymal plasticity and invasion in prostate cancer (PCa). Prostate-specific deletion of Pten and Trp53 in mice resulted in the generation of a mesenchymal tumour cell population expressing nuclear KMT9. We demonstrate that nuclear KMT9 is required for EMT in PCa cells after Pten and Trp53 loss. Mechanistically, we found that KMT9 chromatin occupancy was increased in mesenchymal tumour cells, repressing the expression of key genes for epithelial identity including *Epcam*, *Cdh1* and multiple cytokeratins. Chromatin immunoprecipitation sequencing (ChIP-seq) revealed enrichment of KMT9 at the promoter regions of these essential epithelial "gate-keeper" genes. Functionally, mesenchymal tumour cells displayed a highly invasive and disseminating phenotype in tumour spheroid invasion assays, which was dependent on nuclear KMT9. Importantly, pharmacological inhibition of KMT9 using the highly selective and potent inhibitor KMI169, not only targeted the generation of mesenchymal tumour cells but also and blocked their invasive capacity. Together, our findings uncover KMT9 as a novel EMT regulator and identify a pharmacological approach to specifically target tumour cell plasticity and invasiveness in PCa, paving the way for the future development of KMT9-targeting therapies in cancer.

Keywords: Histone methyltransferase, KMT9, EMT, invasion, prostate cancer.

Introduction

Epitheliums are layers of cells tightly bound to each other through different adhesion molecules and with no motility capacity [1]. During cancer progression, tumour cells undergo molecular and morphological changes, acquiring migratory and invasive features that allow neoplastic cells to disseminate and reach distant organs [2]. Spreading of tumour cells from the primary tumour site to distant secondary organs is the main reason of cancer-related deaths [3]. A pivotal molecular program behind the spreading cascade is the epithelial-mesenchymal transition (EMT), a process where tumour cells gain mesenchymal traits and single-cell dissemination capacity [4]. During EMT, tumour cells undergo a progressive weakening and final loss of cell-cell junctions that results in cell individualization and the establishment of a front-rear polarity axis, promoting tumour invasion and dissemination [5]. Transcription factors from the SNAIL, ZEB and TWIST families have been discovered as master regulators of EMT and associated with cancer progression [3]. These transcription factors promote EMT and invasiveness of normal epithelial cells by repressing the gene expression of essential "gate-keepers" for the epithelial identity such as *Epcam*, *Cdh1* (E-cadherin), and different cytokeratins [6-9]. In cancer, only a subset of tumour cells undergoes EMT and this process is reversible (mesenchymal-epithelial transition, MET). The cellular plasticity results in a broad spectrum of intermediate states between the final epithelial and mesenchymal phenotypes, contributing to tumour heterogeneity and promoting therapy resistance [10, 11].

Pten and *p53* genetic alterations are frequently found in metastatic castration-resistant prostate cancer, driving tumour progression [12-14]. It has been previously reported that prostate epithelial cell-specific deletions of *Pten* and *Trp53* cooperate to promote lethal invasive cancer [15]. A comprehensive phenotypical characterization showed that *Pten* and *Trp53* deletions in prostate epithelium results in aggressive and locally invasive tumours that rapidly progress to lethal sarcomatoid carcinomas [16]. Sarcomatoid tumours have been associated with an EMT phenotype, showing loss of E-cadherin expression [16]. However, metastases are not observed upon loss of *Pten* and *Trp53* in prostate epithelial cells in mouse prostate cancer (PCa) models [15, 16]. Absence of metastatic potential of invasive EMT

tumours have been also reported in murine models of breast cancer [17]. Depletion of *Pten* together with other genetic alterations, such as the conditional activation of *Kras*, has been also reported to contribute to the generation of a subset of $EpCAM^{-}/VIM^{+}$ invasive mesenchymal prostate tumour cells [18]. Despite the increasing number of clinical evidences linking EMT and cancer invasion and progression, there is lack of therapeutic approaches to block EMT at a clinical level [19, 20]. Thus, it is imperative to identify novel upstream druggable regulators of EMT to control cancer aggressiveness [3, 20].

We identified and validated the lysine methyltransferase 9 (KMT9) as a novel target for the treatment of therapy-resistant PCa [21]. KMT9 is an obligatory heterodimer composed of KMT9α and KMT9β that monomethylates histone H4 at lysine 12 (H4K12me1) in PCa and other tumours such as lung, colon, and bladder cancer [21-24]. KMT9 controls transcription of target genes involved in cell cycle regulation thereby promoting tumour cell proliferation. Accordingly, depletion or enzymatic inactivation of KMT9 blocks tumour cell proliferation in prostate, bladder, colorectal and lung cancer [21-24]. Loss of KMT9α in *Pten/Trp53* KO not only blocks prostate tumour growth but also reprograms the tumour immune microenvironment [25]. In addition, KMT9-deficient prostate tumours cells (*Pten/Trp53/Kmt9*α KO) are sensitive to T cell-mediated cytotoxicity and undergo apoptosis whereas KMT9-proficient cells (*Pten/Trp53* KO) are resistant [25]. We also uncovered the presence of KMT9 in mitochondria of prostate tumour cells and demonstrated that mitochondrial KMT9 methylates dihydrolipoamide S-acetyltransferase (DLAT) to control pyruvate dehydrogenase complex (PDC) activity, de novo lipogenesis, and PCa growth [26]. The requirement for KMT9 enzymatic activity to control tumour cell growth identifies KMT9 as an attractive therapeutic target. In consequence, using structure-based drug design, we developed first-in-class, highly potent and selective KMT9 small-molecule inhibitors (KMT9i) that display cellular target engagement with no general cellular toxicity [27, 28]. KMT9 inhibition results in reduced H4K12me1 cellular levels, down-regulation of KMT9 target genes involved in cell cycle regulation, and suppression of tumour cell growth [27]. KMT9 accumulates in the nucleus of

advanced and distant metastatic prostate tumour cells [21] but its contribution to the aggressiveness of advanced PCa remains to be elucidated.

In this work, we used the *Pten*/*Trp53* KO mouse prostate tumour model to assess the impact of KMT9 depletion in PCa invasion. We found that advanced prostate tumours show a subpopulation of mesenchymal tumour cells with high levels of nuclear KMT9 associated to invasive areas. Using mouse model-derived cell lines [25], we show that loss of *Pten and Trp53* in prostate epithelial cells triggers epithelial-mesenchymal transition, generating tumour invasive EpCAM^{-} mesenchymal cells. Our analysis shows that KMT9 drives epithelial-mesenchymal plasticity in *Pten/Trp53* KO prostate tumour cells. At a molecular level, KMT9 regulates the expression of key epithelial gate-keeper genes such as *EpCAM*, *Cdh1* and multiple cytokeratins including *Krt5*, *Krt6A*, *Krt14* and *Krt16*. In *Pten/Trp53* KO cells, KMT9α ablation or treatment with the KMT9 inhibitor KMI169 [27] impaired tumour epithelial-mesenchymal plasticity and blocked tumour cell invasiveness capacity. Taken together, our data show that targeting KMT9 might represent a promising therapeutic avenue with significant clinical benefits for PCa management.

Results

KMT9 promotes EMT and tumour plasticity in Pten/Trp53 KO prostate tumour cells

To explore the role of KMT9 in EMT and PCa invasion, we mated the well-established *PSA-Cre-ER$^{T2(Tg/0)}$/Pten$^{fl/fl}$/Trp53$^{fl/fl}$* mouse PCa model with *PSA-Cre-ER$^{T2(Tg/0)}$/Kmt9$\alpha^{fl/fl}$* mice to generate *PSA-Cre-ER$^{T2(Tg/0)}$/Pten$^{fl/fl}$/Trp53$^{fl/fl}$/Kmt9$\alpha^{fl/fl}$* mice. Then, ten old week mice were treated with tamoxifen to obtain prostate-specific deletions of *Pten/Trp53* and *Pten/Trp53/Kmt9*α. Tumour invasion and presence of tumour mesenchymal cells were evaluated by single cell spatial immunophenotyping 23 weeks upon tamoxifen-induced gene loss using Opal multiplexed immunofluorescence. We included a staining with anti-KRT5 antibody to exclude basal epithelial cells from our analysis [29]. Tumour mesenchymal cells were identified by loss of EpCAM and E-cadherin expression , two widely recognized EMT hallmarks of carcinoma cells [10, 30]. As previously shown, *Pten/Trp53* loss resulted in

advanced adenocarcinomas with presence of prostate intraepithelial neoplasia (PIN) and invasive areas [16], evidenced by the dismantling of the smooth muscle cell layer revealed by anti-SMA staining (Fig. 1A). Importantly, ablation of *Kmt9α* in *Pten/Trp53* KO prostate (resulting in *Pten/Trp53/Kmt9α* KO mice) abolished tumour invasion, limiting PCa progression to the formation of PINs (Fig. 1A). Tumours in *Pten/Trp53* KO prostates were associated with the presence of tumour mesenchymal cells ($EpCAM^-$/E-$cadherin^-$/$KRT5^-$/SMA^-) in PINs but particularly in invasive areas (Fig 1A, B). Importantly, *Kmt9α* loss in *Pten/Trp53* KO prostates significantly resulted in reduced number of mesenchymal tumour cells (Fig. 1A, B).

To uncover the transcriptomic profile of tumour mesenchymal cells, we then performed single-cell RNA sequencing (scRNA-seq) analysis of *Pten/Trp53* KO and *Pten/Trp53/Kmt9α* KO prostates. The unsupervised clustering and two-dimensional embedding using uniform manifold approximation and projection (UMAP) identified nine different cell populations that include 4 different epithelial populations, four stromal populations and a subset of immune cells (Supplementary Fig. 1A). Using the average expression of *Epcam* as threshold, we divided luminal epithelial cells into $Epcam^{high}$ and $Epcam^{low}$ cells (Fig. 1C). Thus, we found that a notably number of luminal epithelial cells in *Pten/Trp53* KO prostates shows low expression of *Epcam* (Fig. 1C). The expression of *Ccnd1*, an *Epcam* target gene [31], was also found reduced in these cells (Fig. 1C). Similar to that found by single cell immunophenotyping (Fig. 1A), $Epcam^{low}$ luminal epithelial cells also showed decreased expression of *Cdh1* (Fig. 1C), highlighting the mesenchymal phenotype of this population. Interestingly, $Epcam^{low}$/$Cdh1^{low}$ luminal epithelial cells showed an increased expression of *Kmt9α* (Fig. 1C). However, the number of $Epcam^{low}$/$Cdh1^{low}$ luminal epithelial cells was found drastically reduced in *Pten/Trp53/Kmt9α* KO prostates (Fig. 1C). Of note, this remaining small population of $Epcam^{low}$/$Cdh1^{low}$ luminal epithelial cells in *Pten/Trp53/Kmt9α* KO prostates showed high expression of *Kmt9α* (Fig. 1C), indicating that only cells where *Kmt9α* ablation was not successful are able to become mesenchymal cells. A similar analysis of a single-cell transcriptional data set from 13 human prostate tumours (GSM4203181[32]) also revealed

presence of *Epcam*^{low}/*Cdh1*^{low} luminal epithelial cells with increased expression of *Kmt9*α (Supplementary Fig. 1B, C).

Next, we performed an immunofluorescence analysis to characterise KMT9α expression in the mesenchymal tumour cell population in *Pten/Trp53* KO prostate tumours using markers for KMT9α, PTEN, p53, EpCAM and SMA. Since *Pten, Trp53*, and *Kmt9*α depletions are driven by CreER^{T2} under control of the prostate-specific PSA promoter, negative cells for these markers were considered as prostate luminal epithelial cells. Our analysis confirmed that in *Pten/Trp53* KO prostates around 30% of tumour cells (PTEN$^-$/p53$^-$/SMA$^-$ cells) are tumour mesenchymal cells (PTEN$^-$/p53$^-$/SMA$^-$/EpCAM$^-$ cells) (Fig. 1D, E). This population was found absent in WT prostates and notably reduced in *Pten/Trp53/Kmt9*α KO prostates (Fig. 1D, E). Of note, the majority of tumour mesenchymal cells in *Pten/Trp53* KO prostates showed nuclear staining of KMT9α (PTEN$^-$/p53$^-$/EpCAM$^-$/nuclear KMT9α^+/SMA$^-$ cells) (Fig. 1F). These data show that depletion of *Pten/Trp53* in mouse prostate epithelial cells is associated with the generation of nuclear KMT9α-expressing tumour mesenchymal cells.

To further decipher the role of KMT9 in EMT, we performed analysis in WT control, *Pten/Trp53* KO and *Pten/Trp53/Kmt9*α KO prostate tumour epithelial cells that have been previously established in our lab [25]. Depletions of PTEN, p53, and KMT9α in cultured cells were confirmed by western blot (Supplementary Fig. 1D). Similar to our observations in vivo flow cytometry analysis performed with *Pten/Trp53* KO cultured cells confirmed the presence of a subpopulation of EpCAM$^-$ prostate epithelial cells that was absent in WT normal prostate cells (Fig. 1G). Importantly, presence of EpCAM$^-$ cells was abolished upon ablation of *Kmt9*α in *Pten/Trp53/Kmt9*α KO cells (Fig. 1G). To rule out the potential presence of cells from non-epithelial origin in *Pten/Trp53* KO cell cultures, we performed lineage staining for leukocyte, endothelial and erythrocyte cell populations using CD45, CD31 and Ter119 markers on these cultured cells (Supplementary Fig. 1E). Thus, flow cytometry analysis confirmed that *Pten/Trp53* KO EpCAM$^-$ cells are lineage (leukocyte, endothelial, erythrocyte) negative cells (Supplementary Fig. 1E). Additionally, presence of EpCAM$^-$ cells was also confirmed in an independent *Pten/Trp53* KO prostate cell population that has been previously described [33]

(Supplementary Fig. 1F). To find out whether nuclear KMT9 drives the generation of EpCAM$^-$ cells, *Pten/Trp53/Kmt9*α KO cells transduced with a nuclear localisation signal (NLS)-tagged KMT9α (*Pten/Trp53/Kmt9*α KO/NLS-KMT9α) were analysed (Supplementary Fig. 1D). Thus, we found that the expression of ectopic nuclear KMT9 in *Pten/Trp53/Kmt9*α KO cells rescued the generation of EpCAM$^-$ cells (Fig. 1H and Supplementary Fig. 1G). Of note, the EpCAM$^-$ cell population was not restored in *Pten/Trp53/Kmt9*α KO transduced cells with a mitochondrial targeting sequence (MTS)-tagged KMT9α (*Pten/Trp53/Kmt9*α KO/MTS-KMT9α) (Supplementary Fig. 1H). These results suggest that nuclear KMT9 might be a molecular switch for the generation of mesenchymal tumour cells in *Pten/Trp53* KO PCa cells.

To further characterize tumour plasticity in *Pten*/*Trp53* KO cells, *Pten/Trp53* KO EpCAM$^+$ and EPCAM$^-$ cells were FACS-sorted and cultured separately (Fig. 1I). After one day, *Pten/Trp53* KO EpCAM$^-$ cells showed a characteristic mesenchymal phenotype with cell-cell adhesion weakening, cell individualization and the establishment of front-back cell polarity (Supplementary Fig. 1I). In contrast, *Pten/Trp53* KO EpCAM$^+$ cells displayed intercellular tight junctions (Supplementary Fig. 1I). After 8 days in cell culture, both *Pten/Trp53* KO EpCAM$^+$ and EpCAM$^-$ sorted cell population showed a mixed phenotype with most of the cells showing tight cell-cell adhesions (Supplementary Fig. 1H). We then analysed these cells by flow cytometry and found that *Pten/Trp53* KO EpCAM$^+$ FACS-sorted cells generated again a subpopulation of EPCAM$^-$ cells (EMT), and vice versa *Pten/Trp53* KO EpCAM$^-$ FACS-sorted cells were now almost 50% EPCAM$^+$ cells, suggesting that these cells can perform mesenchymal-epithelial transition in both directions (Fig. 1J). Together, our findings indicate that KMT9 drives tumour plasticity after Pten/Trp53 loss in prostate cancer.

KMT9 controls the expression of key genes for epithelial identity

We next analysed nuclear KMT9 levels in *Pten/Trp53* KO EpCAM$^+$ and EpCAM$^-$ cells. To that end, subcellular protein fractionation of unsorted *Pten/Trp53* KO, *Pten/Trp53* KO EPCAM$^+$ and EpCAM$^-$ FACS-sorted cells was performed. Thus, we found that cytoplasmic levels of KMT9 were decreased in *Pten/Trp53* KO EpCAM$^-$ cells compared to *Pten/Trp53* KO EpCAM$^+$ cells

(Fig. 2A). However, nuclear and chromatin-bound levels of KMT9 were increased in *Pten/Trp53* KO EpCAM$^-$ cells compared to *Pten/Trp53* KO EpCAM$^+$ cells (Fig. 2A). To unravel the underlying mechanisms of tumour cell plasticity regulation by KMT9, we performed a global transcriptome analysis (RNA-seq) of *Pten/Trp53* KO EpCAM$^+$ and *Pten/Trp53* KO EpCAM$^-$ FACS-sorted cells and chromatin immunoprecipitation sequencing (ChIP-seq) of *Pten/Trp53* KO cells. In total, we found 1277 differentially expressed genes (DEGs) when comparing *Pten/Trp53* KO EpCAM$^+$ and *Pten/Trp53* KO EpCAM$^-$ FACS-sorted cells, and 13042 genes with KMT9α-specific peaks at gene promoter regions in *Pten/Trp53* KO cells (Fig. 2B). Overlapping of the 1277 DEGs and the 13042 genes with peaks at promoter regions identified 760 direct KMT9 target genes (Fig. 2B). To gain insight into the shared biological functions of these 760 direct KMT9 target genes, we performed a Gene Ontology (GO) enrichment analysis for biological processes. Among the top-ranking categories, the gene sets were predominantly involved in regulation of cell migration and communication, tissue development and cell adhesion (Fig. 2C), all of which are biological processes closely associated with EMT [5]. Accordingly, among the DEGs in the enriched gene sets we found a strong downregulation of key epithelial "gate-keepers" such as *Epcam*, *Cdh1*, *Krt5, Krt6a, Krt14* and *Krt16* in *Pten/Trp53* KO EpCAM$^-$ FACS-sorted cells compared to *Pten/Trp53* KO EpCAM$^+$ FACS-sorted cells (Fig. 2D, E). All these genes showed KMT9α enrichment at their respective promoter regions (Fig. 2E), highlighting the direct regulatory role of KMT9. Differential expression of *Epcam*, *Cdh1* and different cytokeratins (*Krt4*, *Krt5*, *Krt6a*, *Krt7*, *Krt8*, *Krt14*, *Krt16*, and *Krt18*) between *Pten/Trp53* KO EPCAM$^+$ and *Pten/Trp53* KO EPCAM$^-$ cells was validated by RT-qPCR (Fig. 2F). The expression of the EpCAM target gene *Ccnd1* [31] was also found downregulated in *Pten/Trp53* KO EPCAM$^-$ cells (Fig. 2F). EpCAM loss in *Pten/Trp53* KO EpCAM$^-$ cells was confirmed in western blot analysis using antibodies targeting the extracellular (EpEx) and intracellular (EpICD) domains (Fig. 2G). In line with our transcriptomic data, loss of EpCAM was associated with loss of other crucial epithelial markers such as E-cadherin and cytokeratin 5, and decreased expression of its target gene cyclin D1 (Fig. 2G). β-catenin, a crucial component of adherent junctions and plays a key role in maintaining cellular polarity [34], was

not found differentially regulated at RNA levels (Supplementary Fig. 2A). However, β-catenin protein levels were found strongly decreased in EPCAM$^-$ cells compared to unsorted *Pten/Trp53* KO and *Pten/Trp53* KO EpCAM$^+$ cells (Fig. 1G). Proficiency or deficiency of PTEN, p53 and KMT9α in sorted and unsorted cells was confirmed by western blot (Supplementary Fig. 2B). We next aimed to confirm the KMT9-dependant regulation of these key epithelial genes by analysing their expression by in WT, *Pten/Trp53* KO, *Pten/Trp53/Kmt9α* KO, and *Pten/Trp53/Kmt9α* KO/NLS-KMT9α cells. Thus, depletion of *Kmt9α* in *Pten/Trp53/Kmt9α* KO cells compared to *Pten/Trp53* KO cells resulted in significantly increased expression of *Epcam*, *Cdh1*, *Krt5*, *Krt6A*, *Krt14*, *Krt16*, and *Ccnd1* (Fig. 2H, Supplementary Fig. 2C). In contrast, ectopic expression of nuclear KMT9 in *Pten/Trp53/Kmt9α* KO/NLS-KMT9α significantly decreased the expression of *Epcam*, *Krt5*, *Krt6A*, *Krt14*, *Krt16*, and *Ccdn1* (Fig. 2H, Supplementary Fig. 2C). These findings were further supported by western blot analysis showing increased expression of EpCAM, E-cadherin, cytokeratin 5 and cytokeratin 6A in *Pten/Trp53/Kmt9α* KO cells when compared to *Pten/Trp53* KO cells (Fig. 2J). In contrast, ectopic expression of nuclear KMT9α in *Pten/Trp53/Kmt9α* KO/NLS-KMT9α resulted in a notably reduction in the expression of these genes and the EpCAM target gene cyclin D1 (Fig. 2I). Of note, mRNA expression of β-catenin (*Ctnnb1*) was not regulated by KMT9 (Supplementary Fig. 2D).

Next, we wondered whether the EpCAM$^-$ cell population observed in *Pten/Trp53/Kmt9α* KO/NLS-KMT9α cells (Fig.1H and Supplementary Fig. 1G) also shows decreased expression of epithelial "gatekeeper" proteins. Similarly to that found in *Pten/Trp53* KO EpCAM$^-$ cells, rescue of EpCAM$^-$ cells after nuclear KMT9 ectopic expression in *Pten/Trp53/Kmt9α* KO cells resulted in decrease expression levels of EpCAM, E-cadherin, cytokeratin 5, β-catenin, and cyclin D1 (Fig. 2J). Together, our data show that KMT9 represses the expression of key EMT genes and it is essential for the generation of tumour mesenchymal cells in *Pten/Trp53* KO PCa cells.

KMT9 drives the generation of invasive tumour mesenchymal cells in PCa

When cells undergo EMT, epithelial organoids typically stop growing, disintegrate, or fail to form properly. This arrest in growth occurs due to several fundamental biological changes that happen during EMT such as disruption of cell-to-cell adhesion or loss of stemness and progenitor identity [35]. Thus, we established organoid cultures with *Pten/Trp53* KO unsorted cells, *Pten/Trp53* KO EpCAM$^+$ and *Pten/Trp53* KO EpCAM$^-$ FACS-sorted cells to explore the properties of these cells (Fig. 3A). We found that *Pten/Trp53* KO unsorted and *Pten/Trp53* KO EPCAM$^+$ cells grew as organoids (Fig. 3A). In contrast, *Pten/Trp53* KO EpCAM$^-$ cells did not grow as organoids and showed an invasive phenotype, displaying the typical front-rear polarity of EMT cells (Fig. 3A). As a result of cell growth over time, *Pten/Trp53* KO EpCAM$^+$ cells left the Matrigel dome growing as a compact 2D layer with tight intercellular junctions (Fig. 3B). However, *Pten/Trp53* KO EpCAM$^-$ cells showed a high disseminating capacity to long distances with cell individualization and front-rear polarity (Fig. 3B). *Pten/Trp53* KO unsorted cells showed a mixed phenotype with compact growth and disseminated cells (Fig. 3B). These results then prompted us to evaluate the migratory and invasive capacities of *Pten/Trp53* KO EpCAM$^-$ cells. Thus, to study collective migration and dissemination, 2-days spheroids were inserted into the central channel of a chemotaxis chamber and a right-to-left chemoattracting gradient was created (Supplementary Fig. 3A). After 3 days, whereas most of *Pten/Trp53* KO unsorted and *Pten/Trp53* KO EpCAM$^+$ cells migrated collectively, *Pten/Trp53* KO EpCAM$^-$ cells showed a high disseminating ability (Supplementary Fig. 3A, B). Tumour spheroid invasion assays not only confirmed this disseminating phenotype but also showed a massive invasive ability of *Pten/Trp53* KO EpCAM$^-$ cells compared to *Pten/Trp53* KO unsorted and *Pten/Trp53* KO EpCAM$^+$ cells (Fig. 3C, D and Supplementary video 1, 2, 3). In contrast, the spheroid growth rate was very similar among the three different cellular types (Fig. 3E). Next we wondered whether the EpCAM$^-$ cell population observed in *Pten/Trp53/Kmt9*α KO/NLS-KMT9α upon ectopic expression of NLS-KMT9α in *Pten/Trp53/Kmt9*α KO cells (Fig.1H and Supplementary Fig. 1G) also displays disseminating and invasive capacities. To this end, we performed spheroid tumour invasion assay with *Pten/Trp53/Kmt9*α KO/NLS-KMT9α unsorted and *Pten/Trp53/Kmt9*α KO/NLS-KMT9α EpCAM$^+$ and *Pten/Trp53/Kmt9*α KO/NLS-KMT9α

EpCAM$^-$ FACS-sorted cells. Importantly, *Pten/Trp53/Kmt9*α KO/NLS-KMT9α EpCAM$^-$ cells displayed high disseminating and invasive capacity when compared to unsorted *Pten/Trp53/Kmt9*α KO/NLS-KMT9α and *Pten/Trp53/Kmt9*α KO/NLS-KMT9α KO EpCAM$^+$ cells (Fig. 3F, G). Of note, the spheroid growth rate was very similar among all three different cellular types (Fig. 3H). Taken together, our findings further demonstrate that nuclear KMT9 drives the generation of highly invasive prostate tumour mesenchymal cells.

Pharmacological inhibition of KMT9 impairs EMT and blocks invasion in *Pten/Trp53* KO prostate cells

We have recently reported the development of a potent and selective inhibitor of the KMT9 histone methyltransferase activity (KMI169) with anti-proliferative effects in PCa [27]. To assess cellular target engagement of KMI169 in *Pten/Trp53* KO, we performed Cellular Thermal Shift Assays (CETSA) [36]. Thereby, we revealed strong stabilization of endogenous KMT9 (ΔT_m=3.25°C) compared to DMSO (Fig. 4A, B). These results demonstrate cell membrane permeability and cellular target engagement of KMI169 making the inhibitor a suitable tool to study cellular KMT9 functions in *Pten/Trp53* KO cells. To address the cellular consequences of KMT9 inhibition in cells, *Pten/Trp53* KO cells were cultured in presence of either vehicle or KMI169. Our flow cytometry analysis shows that pharmacological targeting of KMT9 with KMI169 significantly impaired EMT in *Pten/Trp53* KO cells (Fig. 4C and D), further supporting that the histone methyltransferase activity of KMT9 is essential for regulating tumour cell plasticity in *Pten/Trp53* KO cells. Mechanistically, we show that inhibition of the KMT9 enzymatic activity results in the upregulation of markers of epithelial identity that were found highly downregulated in *Pten/Trp53* KO EpCAM$^+$ and *Pten/Trp53/Kmt9*α KO/NLS-KMT9α EpCAM$^-$ cells (Fig. 2D-J and Fig. 4E). To further validate that KMT9 enzymatic activity does not only impair the generation of tumour mesenchymal cells but also directly affects tumour mesenchymal invasive capacity, we performed tumour spheroid invasion assays with KMI169. Vehicle or KMI169-treated tumour spheroids were embedded in Matrigel and invasion was assessed. Importantly, we found that KMT9 inhibition blocks the invasive behaviour of

Pten/Trp53 KO EpCAM$^-$ cells (Fig. 4F, G). This effect was specific for invasion since at that concentration KMI169 did not affect the tumour spheroid size (Fig. 4H). Altogether, these data indicate that targeting KMT9 might be a valuable therapeutic strategy to impair tumour cell plasticity and invasiveness in PCa.

Discussion

EMT is a highly dynamic and reversible process where epithelial cells are transformed into mesenchymal cells with the generation of many transitioning partial states [37]. Dysregulation of this evolutionarily conserved program has been extensively reported during cancer progression, increasing invasiveness, metastatic dissemination and therapy resistance of tumour cells [38]. Although regulatory networks behind the balance between epithelial and mesenchymal states are still not fully understood, pre-existing or acquired genetic and epigenetic alterations during tumour progression can drive EMT plasticity in cancer [39]. This cellular reprogramming is tightly regulated by different families of EMT-associated transcription factors (EMT-TF) that includes SNAIL, ZEB, TWIST and SOX [40]. A major consequence of EMT-TF activity is the suppression of genes required to preserve epithelial architecture and identity, including EpCAM, Cdh1 and cytokeratins [41-43], what results in the acquisition of migrative and invasive phenotypes. The identification of novel regulators that control the stability and reversibility of epithelial and mesenchymal states is essential to understand how EMT plasticity contributes to tumour progression.

We have previously reported that KMT9 is a novel histone methyltransferase that controls cell proliferation in PCa and accumulates in the nucleus of advanced and distant metastatic human prostate tumours [21] but how KMT9 might promote tumour progression remains unknown so far. Our findings identify KMT9 as an upstream epigenetic regulator of EMT, thereby extending the current framework of EMT regulation beyond the canonical EMT-inducing transcription factors. KMT9 regulates the expression of critical epithelial “gatekeeper” genes that are necessary to maintain epithelial identity. These findings suggest that KMT9 may act at an additional regulatory layer upstream of, or in parallel with the classical EMT transcriptional

network. This is particularly relevant in the context of prostate tumorigenesis driven by Pten and Trp53 loss. Genetic ablation of these tumour suppressors increases tumour heterogeneity by generating a small subset of cells that acquire mesenchymal characteristics. Of note, the generation of a subset of tumour mesenchymal cells has been also previously reported in Pten KO/ $Kras^{G12D}$ prostate cancer cells [18]. Although carcinomas are classified into poorly or well-differentiated tumours, the majority are equilibrated composites of epithelial and mesenchymal phenotypes [39]. Our data show that KMT9 controls a transcriptional repression program of key genes for the maintenance of epithelial identity such as E-cadherin. Thus, KMT9 drives the generation of tumour mesenchymal cells in prostate epithelial cells after Pten and Trp53 loss. KMT9 therefore represents an important component of the molecular network that contributes via epigenetic regulation to retain the epithelial identity or acquire more mesenchymal and invasive properties.

Acquisition of mesenchymal features has long been associated with increased migratory and invasive capacity. EMT-TFs can promote invasion through coordinated changes in cell adhesion, cytoskeletal organization, and extracellular matrix interactions [7, 44, 45]. In this regard, epigenetic mechanisms are particularly well suited to regulate such plasticity because they can establish and maintain transcriptional states while remaining reversible in response to cellular or environmental cues. Here, our findings provide functional evidence linking KMT9 to tumour cell invasion at two different levels. Our data demonstrate that KMT9 epigenetic regulation controls both the generation of tumour cells with mesenchymal phenotype and the invasive behaviour of mesenchymal prostate cancer cells after *Pten/Trp53* loss.

Despite the well-established contribution of EMT to tumour progression and invasion, therapeutically targeting this process remains challenging. Targeting EMT-TFs is challenging because of their structural and physicochemical properties, so they have been traditionally considered as “undruggable”. We previously reported the first inhibitor of KMT9 methyltransferase activity [27], providing a valuable tool to pharmacologically interrogate the role of KMT9 in epithelial–mesenchymal plasticity. Inhibition of KMT9 promotes the expression of epithelial markers, including EpCAM, E-cadherin, and multiple cytokeratins, consequently

reducing the abundance of mesenchymal tumour cells. Importantly, this effect extends beyond molecular reprogramming since KMT9 inhibition also suppresses the invasive capacity of the mesenchymal tumour cell population. Taken together, these findings provide a novel mechanism where KMT9 acts as a molecular switch that connects epithelial identity, mesenchymal plasticity and invasive behaviour in PCa.

Methods

Multiplexed immunofluorescence analysis

Mouse prostate tissues were fixed in 4% paraformaldehyde and embedded in paraffin. Tissue sections (5 µm) were deparaffinized by heating slides at 55-60°C followed by xylene and ethanol gradient (100%, 95%, 70%, 50%, 30% and H2O) incubations. Opal 7-colour kit (Akoya Biosciences) was used to perform multiplex immunofluorescence according to the manufacturer's instructions. Briefly, antigen retrieval was conducted by heating sections in either AR6 or AR9 buffer in a pressure cooker for 20 min. Then, samples were blocked with Antibody Diluent for 10 min at RT and incubated sequentially with two different panels of primary antibodies (Table 1) followed by secondary antibody and Opal fluorophore incubations and antibody removal. After all sequential immunofluorescence staining, DAPI staining was performed and slides were mounted with Fluoromount. Finally, PhenoImager™ Fusion (Akoya Biosciences) was used for image acquisition and QuPath software for protein expression and distribution analysis in prostate samples.

RNA sequencing (RNA-seq)

RNA from mouse prostate was isolated using the RNeasy Plus Mini kit (Qiagen) essentially as described by the manufacturer. RNA sequencing was performed by Novogene UK Ltd. using standard Illumina protocols to generate raw data (.fastq files). Reads were aligned to the mm10 mouse genome assembly using STAR version 2.7.11b. The aligned reads were counted with the Homer 5.1 software with default settings (analyzeRepeats.pl) and differentially expressed

genes were identified using EdgeR 4.8.2. Heatmaps were generated using Morpheus (https://software.broadinstitute.org/morpheus/). Data are deposited under GSE350577.

Single-cell mRNA sequencing (scRNA-seq)

We used and analysed the scRNA-seq data from GSE253017 [25] and GSM4203181).To define $EpCAM^{high}$ and $EpCAM^{low}$ values, the 25th percentile of EpCAM expression was calculated; values below this threshold were classified as low, while those above were classified as high.

Chromatin immunoprecipitation sequencing (ChIP-seq)

The ChIP-seq seq data GSE313620 were used for the analysis. Reads were aligned to the mm10 mouse genome assembly using Bowtie2 [46]. Peak calling was subsequently performed with the MACS algorithm (v1.4.2) [60] using input as control. All peaks with a false discovery rate (FDR) greater than 5 % were excluded from further analysis. The resulting reads were used to generate genome-wide intensity profiles, which were visualized using the Integrative Genomics Viewer (IGV) browser[61]. HOMER[62] was used to annotate peaks (annotatePeaks.pl). The genomic features (promoter, exon, intron, 3'UTR, and intergenic regions) bases on Refseq annotation.

Cell culture

Mouse prostate epithelial cell cultures were established as previously described [25]. Cells were cultured with mouse prostate cancer medium (mPCM): advanced DMEM/F12 supplemented with Advanced DMEM/F-12 culture medium supplemented with HEPES 10mM, B-27 1x, glutamine 2 mM, N-acetyl-L-cysteine 1.25 mM, murine EGF 50 ng/µl, murine Noggin 100 ng/ml, murine R-Spondin-1 500 ng/ml, A83-01 200 nM, DHT 1 nM and Y-37632 10µM.

Flow cytometry and FACS

Mouse prostate epithelial cells were stained with Zombie NIR (Biolegend) for 20 min at RT to rule out dead cells. Cells were washed with 1 x PBS, 0.5% BSA (Sigma-Aldrich) (cytometry staining buffer, CSB) and incubated for 20 min at 4°C in with anti-EpCAM-FITC (118208, Biolegend, lot: B288878, 1/200), anti-EpCAM-BV605 (118227, Biolegend, lot: B361885, 1/80), anti-CD45-FITC (11-0451-82, eBioscience, lot: 2015744, 1/100), anti-CD31-FITC (11-0311-82, eBioscience, lot: 4330484, 1/50), anti-Ter-119-FITC (11-5921-85, eBioscience, lot: 2056566, 1/200) and anti-CD49f-PE (313612, Biolegend, lot: B274785, 1/20). Cells were washed with CBS and immunofluorescence was acquired with a BD LSRFortessa cytometer (BD Bioscience) and analysed with FloJo software (BD Bioscience). $EpCAM^+$ and $EpCAM^-$ cells were isolated by Fluorescence-activated Cell Sorting (FACS) using CytoFlex SRT Cell Sorter (Beckman Coulter).

Western blot analysis

Mouse prostate cells were lysed on ice using RIPA buffer (1 mM EDTA, 50 mM Tris-HCl pH7.5, 0.1% SDS, 150 mM NaCl, 1% NP40, 1% NaDeoxycholate) and centrifuged at 14.000 rpm for 10 min. Subcellular protein fractionation was performed with the Subcellular Protein Fractionation Kit for Cultured Cells (Thermo Scientific), according to manufacturer´s instructions. Protein concentration was quantified by Bradford (Bio-Rad). SDS-PAGE electrophoresis was conducted to separate proteins that were transferred to a PVDF membrane (Millipore). Then, membranes where blocked and incubated with the corresponding primary and secondary antibodies: anti-PTEN (9552, Cell Signaling, lot: 3; 1:1000), anti-TRP53 (LIN-P956, Linaris, lot: 6067079; 1:2000), anti-KMT9α (228445, Schüle Lab, lot: 27112018; 1:500), anti-H4K12me1 (27429, Biogenes. lot 121217; 1:1000), anti-H4 (ab10158, Abcam, lot: GR3226771-1; 1:3000); anti-EpCAM (EpEx) (21050-1-AP, Proteintech, lot. 00044849; 1:1000), anti-EpCAM (EpICD) (93790, Cell signaling, lot: 3; 1:1000), anti-E-cadherin (610182 BD, lot: 4050815; 1:1000), anti-β-catenin (610154, BD, lot: 5251449; 1:2000), anti-Cytokeratin 5 (orb229186, biorbyt, lot: DP6921; 1:500), anti-Cyclin D1 (MA5-14512 ThermoFisher, lot: WC3224321; 1:1000), anti-Tubulin (T6074, Sigma, lot: 0000127282, 1:10000). Finally,

corresponding HRP-conjugated secondary antibodies were used and chemiluminescence signal was detected using X-ray films (Fujifilm) and developed with an automated film processor (Curix 60, Agfa).

RNA preparation for quantitative RT-PCR analysis

Total RNA was isolated from prostate epithelial cells using the RNeasy Plus Mini Kit (Qiagen) according to manufacturer´s instructions and concentration was measured using Nanodrop. RT-PCR was performed using SuperScript II Reverse Transcriptase (Invitrogen) kit and qPCR using Absolute qPCR SYBR Green ROX Mix (Thermo Scientific) following manufacturer´s instructions. The following gene specific primer pairs were used: *EpCAM* 5´-gcggctcagagagactgtg-3´and 5´-ccaagcatttagacgccagttt-3´; *Cdh1* 5´-caggtctcctcatggctttgc-3´and 5´-cttccgaaaagaaggctgtcc-3´; *Ccnd1* 5´-gcgtaccctgacaccaatctc-3´and 5´-ctcctcttcgcacttctgctc-3´; *Krt4* 5´-ctgagggactaccaggctct-3´and 5´-cagaaccggagcaaaaaccg-3´; *Krt5* 5´-aacgtcaagaagcagtgtgc-3´and 5´-tccagctctgtcagcttgtt-3; *Krt6a* 5´-ctgaggaacatgcaggacac-3´and 5´-ctacatccttcttcagggtcacg-3´; *Krt7* 5´- cgcaacacccggaatgagat-3´and 5´-tggactctaacttggcacgc-3´; *Krt8* 5´-gttgtccatgttgctcctcg-3´and 5´-gtgaaccagagcctgttgag-3´; *Krt14* 5´-agcggcaagagtgagatttct-3´and 5´- cctccaggttattctccaggg-3´; *Krt16* 5´-tgagctgaccctgtccaga-3´and 5´-ctcaaggcaagcatctcctc-3´; *Krt18* 5´-cgaggcactcaaggaagaac-3´and 5´-cttggtggtgacaactgtgg-3; *Polr2a* 5'-caccccagcttctcccaaat-3' and 5'-agtatgtcggggaggttgga-3';

Immunofluorescence of organoids

Round coverslips were placed on the bottom of 24-well plates and 10.000 unsorted, $EpCAM^+$ or $EpCAM^-$ *Pten/Trp53* KO cells were seeded per well embedded in 40 μl Matrigel domes and cultured for 5 days in mPCM. Before starting the immunofluorescence protocol, images of migrative/invasive cells at the border of Matrigel domes were taken. Then, organoids were stained as previously described [47]. Briefly, organoids were fixed with 4% PFA in PME buffer (PIPES 500 nM, MgCl2 25 mM, EDTA 50 mM) for 20 min at RT. Organoids were washed with

IF buffer (Triton X-100 0.2%, Tween 0.05% PBS) and incubated for 30 min at RT in permeabilization buffer (0.5% Triton X-100 PBS). After washing with IF buffer, organoids were blocked for 30 min at RT and incubated with the primary antibody (EpCAM (ICD), 93790, Cell Signaling) overnight at 4°C. Then secondary Alexa Fluor 488 goat anti-rabbit (A11034, Molecular Probes) and Alexa Fluor Plus 647 phalloidin (A30107, Invitrogen) were added for 1h at RT. Finally, DAPI (1 μg/ml) was used to stain nuclei for 5 min and immunofluorescence was assessed using the Zeiss Axio Observer.Z1 microscope.

Cellular Thermal Shift Assay (CETSA)

For CETSA, Pten/Trp53 KO cells were incubated with 500 nM of KMI169 or KMI169Ctrl for 24 hours. Then, cells were washed, harvested using trypsin, and pelleted by centrifugation. The pellet was washed twice with PBS supplemented with cOmplete™ EDTA-free Protease Inhibitor Cocktail (Roche) and Phosphatase Inhibitor Cocktail 2 and 3 (Sigma) and divided into 16 aliquots of 40 µl containing 200,000 cells. Cells were then frozen in liquid nitrogen and thawed at 25 °C three times and each aliquot was heated to a defined temperature by applying a gradient between 40 °C and 70 °C in a PCR cycler (Mastercycler Nexus Gradient, Eppendorf; 16-well gradient, 55 °C ± 15). After 3 min incubation, aliquots were snap frozen in liquid nitrogen and thawed at 25 °C. Cell lysates were centrifuged at 20000x g (4 °C) for 20 minutes. Supernatants were mixed with 5x loading buffer, heated to 95 °C for 5 min, and analysed by Western blotting. Chemiluminescent signals were recorded with an Amersham imager 600 (GE Healthcare) and quantified using Amersham imager 600 1.2.0 software. Calculation of ΔTm was conducted using sigmoidal model in GraphPad Prism 6.0.

Spheroid invasion assay

Prostate epithelial cell monolayers were dissociated, harvested and resuspended in mPCM to obtain 2 x 10^4 cells/ml. Then, 200 µl/well were seeded in presence or DMSO or KMI169 into ultra-low attachment 96-well round bottom plates (Corning) and cells were incubated at 37 °C, 5% CO_2 for 2 days. Spheroid formation was visually confirmed and 100 µl/well were gently

removed. Next, 100 µl of Matrigel or Matrigel with 2x vehicle or KM169 treatment were gently added into the U-bottom wells. Image acquisition was performed every 2-3 days using the Zeiss Axio Observer.Z1 microscope or Incucyte S3 Live-Cell Analysis System. Batch segmentation of a pool of imaging was used to quantify spheroid invasion by using shadow machine learning with QuPath software. Invasiveness videos were made acquiring images every 3h with Incucyte S3 Live-Cell Analysis System.

Spheroid migration assay

Tumour spheroids were formed for 2 days as previously described for spheroid invasion assays. Cell migration was assessed by using the µ-Slide Chemotaxis (Ibidi) following manufacturer's instructions. Briefly, 6 µl of medium containing a 2 days spheroid were added to the central channel of the slide. The position of the spheroid inside the channel was controlled with a microscope. Both side reservoirs were filled with 65 µl of chemoattractant-free medium (Advanced DMEM/F12 medium). Then, one of the side reservoirs was filled with 30 µl of chemoattractant (mPCM 5%FCS; final concentration: 1:2 mPCM 5%FCS). Images were taken every day for 3 days using the Zeiss Axio Observer.Z1 microscope. Individual cells and small clusters of cells were quantified as EMT cells using ImageJ software.

Mouse studies

For the in vivo studies, PSA-Cre-ER$^{T2(Tg/0)}$/Pten$^{fl/fl}$/Trp53$^{fl/fl}$, PSA-Cre-ER$^{T2(Tg/0)}$/Pten$^{fl/fl}$/Trp53$^{fl/fl}$/Kmt9$\alpha^{fl/fl}$, and PSA-Cre-ER$^{T2(Tg/0)}$–mice were employed. All animals were maintained in the pathogen-free barrier facility at the University Medical Center Freiburg under institutional animal welfare regulations and with approval from the Regierungspräsidium Freiburg (35-9185.81/G-19/26). Mice were kept under controlled temperature and humidity conditions on a 12-h light/dark cycle, with unrestricted access to water and either standard rodent chow (3807, granovit, Kaiseraugst, Switzerland) or a tamoxifen citrate-containing diet (400 mg/kg; A115T70400, ssniff, Soest, Germany). At the end of the experimental procedures,

animals were euthanized by cervical dislocation, and the tissues were promptly collected and processed for subsequent analyses

Statistics

At least three independent experiments were performed with comparable results. Data are represented as mean +/- standard deviation (s.d.) as indicated. Significance was calculated by unpaired Student T test as indicated in the figure legends. Sample sizes and p values are indicated where appropriate.

Author contributions

E.M., R.S. and J.P. generated the original hypothesis. J.P., L.P., S.W., F.P., S.U., M.S., A.R. performed experiments. D.W. performed bioinformatics analyses. M.J. and D.M. provided logistic and technical support. J.P. and E.M. took primary responsibility for writing the manuscript. All authors edited the manuscript.

Acknowledgments

We thank the Lighthouse Core Facility staff of the Medical Center University of Freiburg for helping with cell sorting, flow cytometry, and single-cell spatial phenotype resources and their excellent support. We are thankful to R. Romero for providing prostate cancer cells. Lighthouse Core Facility is funded in part by the Medical Faculty, University of Freiburg (Project Numbers 2023/A2-Fol; 2021/B3-Fol), the DKTK, and the DFG (Project ID 450392965). E.M. was supported by the DKTK grants FR01-374 and FR01-SOB-KMT9Pro-MTZ. This work was also funded by the Deutsche Forschungsgemeinschaft (DFG, German Research Foundation)-SFB1479 ID: 441891347-P20N and Project ID: 587387648 to E.M.; Project-ID 1059002051 Schu688/15-1, Schu688/18-1, SFB 992 (Project-ID: 192904750), and CIBBS Germany´s Excellence Strategy-EXC- 2189-Project ID: 390939984 to R.S; Project ID: 587387648 to M.J.

Competing interests

The authors declare no competing interests.

References

[1] P.W. Miller, D.N. Clarke, W.I. Weis, C.J. Lowe, W.J. Nelson, The evolutionary origin of epithelial cell-cell adhesion mechanisms, Curr Top Membr, 72 (2013) 267-311.

[2] P. Friedl, K. Wolf, Tumour-cell invasion and migration: diversity and escape mechanisms, Nat Rev Cancer, 3 (2003) 362-374.

[3] H. Zheng, Y. Kang, Multilayer control of the EMT master regulators, Oncogene, 33 (2014) 1755-1763.

[4] J. Bastid, EMT in carcinoma progression and dissemination: facts, unanswered questions, and clinical considerations, Cancer Metastasis Rev, 31 (2012) 277-283.

[5] S. Lamouille, J. Xu, R. Derynck, Molecular mechanisms of epithelial-mesenchymal transition, Nat Rev Mol Cell Biol, 15 (2014) 178-196.

[6] E. Batlle, E. Sancho, C. Franci, D. Dominguez, M. Monfar, J. Baulida, A. Garcia De Herreros, The transcription factor snail is a repressor of E-cadherin gene expression in epithelial tumour cells, Nat Cell Biol, 2 (2000) 84-89.

[7] A. Cano, M.A. Perez-Moreno, I. Rodrigo, A. Locascio, M.J. Blanco, M.G. del Barrio, F. Portillo, M.A. Nieto, The transcription factor snail controls epithelial-mesenchymal transitions by repressing E-cadherin expression, Nat Cell Biol, 2 (2000) 76-83.

[8] C. Vannier, K. Mock, T. Brabletz, W. Driever, Zeb1 regulates E-cadherin and Epcam (epithelial cell adhesion molecule) expression to control cell behavior in early zebrafish development, J Biol Chem, 288 (2013) 18643-18659.

[9] S. Guaita, I. Puig, C. Franci, M. Garrido, D. Dominguez, E. Batlle, E. Sancho, S. Dedhar, A.G. De Herreros, J. Baulida, Snail induction of epithelial to mesenchymal transition in tumor cells is accompanied by MUC1 repression and ZEB1 expression, J Biol Chem, 277 (2002) 39209-39216.

[10] O. Gires, M. Pan, H. Schinke, M. Canis, P.A. Baeuerle, Expression and function of epithelial cell adhesion molecule EpCAM: where are we after 40 years?, Cancer Metastasis Rev, 39 (2020) 969-987.

[11] J. Yang, P. Antin, G. Berx, C. Blanpain, T. Brabletz, M. Bronner, K. Campbell, A. Cano, J. Casanova, G. Christofori, S. Dedhar, R. Derynck, H.L. Ford, J. Fuxe, A. Garcia de Herreros, G.J. Goodall, A.K. Hadjantonakis, R.Y.J. Huang, C. Kalcheim, R. Kalluri, Y. Kang, Y. Khew-Goodall, H. Levine, J. Liu, G.D. Longmore, S.A. Mani, J. Massague, R. Mayor, D. McClay, K.E. Mostov, D.F. Newgreen, M.A. Nieto, A. Puisieux, R. Runyan, P. Savagner, B. Stanger, M.P. Stemmler, Y. Takahashi, M. Takeichi, E. Theveneau, J.P. Thiery, E.W. Thompson, R.A. Weinberg, E.D. Williams, J. Xing, B.P. Zhou, G. Sheng, E.M.T.I. Association, Guidelines and definitions for research on epithelial-mesenchymal transition, Nat Rev Mol Cell Biol, 21 (2020) 341-352.

[12] C.S. Grasso, Y.M. Wu, D.R. Robinson, X. Cao, S.M. Dhanasekaran, A.P. Khan, M.J. Quist, X. Jing, R.J. Lonigro, J.C. Brenner, I.A. Asangani, B. Ateeq, S.Y. Chun, J. Siddiqui, L. Sam, M. Anstett, R. Mehra, J.R. Prensner, N. Palanisamy, G.A. Ryslik, F. Vandin, B.J. Raphael, L.P. Kunju, D.R. Rhodes, K.J. Pienta, A.M. Chinnaiyan, S.A. Tomlins, The mutational landscape of lethal castration-resistant prostate cancer, Nature, 487 (2012) 239-243.

[13] R.J. Rebello, C. Oing, K.E. Knudsen, S. Loeb, D.C. Johnson, R.E. Reiter, S. Gillessen, T. Van der Kwast, R.G. Bristow, Prostate cancer, Nat Rev Dis Primers, 7 (2021) 9.

[14] L.F. van Dessel, J. van Riet, M. Smits, Y. Zhu, P. Hamberg, M.S. van der Heijden, A.M. Bergman, I.M. van Oort, R. de Wit, E.E. Voest, N. Steeghs, T.N. Yamaguchi, J. Livingstone, P.C. Boutros, J.W.M. Martens, S. Sleijfer, E. Cuppen, W. Zwart, H.J.G. van de Werken, N. Mehra, M.P. Lolkema, The genomic landscape of metastatic castration-resistant prostate cancers reveals multiple distinct genotypes with potential clinical impact, Nat Commun, 10 (2019) 5251.

[15] Z. Chen, L.C. Trotman, D. Shaffer, H.K. Lin, Z.A. Dotan, M. Niki, J.A. Koutcher, H.I. Scher, T. Ludwig, W. Gerald, C. Cordon-Cardo, P.P. Pandolfi, Crucial role of p53-dependent cellular senescence in suppression of Pten-deficient tumorigenesis, Nature, 436 (2005) 725-730.

[16] P. Martin, Y.N. Liu, R. Pierce, W. Abou-Kheir, O. Casey, V. Seng, D. Camacho, R.M. Simpson, K. Kelly, Prostate epithelial Pten/TP53 loss leads to transformation of multipotential progenitors and epithelial to mesenchymal transition, Am J Pathol, 179 (2011) 422-435.

[17] R.D. Cardiff, The pathology of EMT in mouse mammary tumorigenesis, J Mammary Gland Biol Neoplasia, 15 (2010) 225-233.

[18] M. Ruscetti, B. Quach, E.L. Dadashian, D.J. Mulholland, H. Wu, Tracking and Functional Characterization of Epithelial-Mesenchymal Transition and Mesenchymal Tumor Cells during Prostate Cancer Metastasis, Cancer Res, 75 (2015) 2749-2759.

[19] W. Lu, Y. Kang, Epithelial-Mesenchymal Plasticity in Cancer Progression and Metastasis, Dev Cell, 49 (2019) 361-374.

[20] H.L. Ang, C.D. Mohan, M.K. Shanmugam, H.C. Leong, P. Makvandi, K.S. Rangappa, A. Bishayee, A.P. Kumar, G. Sethi, Mechanism of epithelial-mesenchymal transition in cancer and its regulation by natural compounds, Med Res Rev, 43 (2023) 1141-1200.

[21] E. Metzger, S. Wang, S. Urban, D. Willmann, A. Schmidt, A. Offermann, A. Allen, M. Sum, N. Obier, F. Cottard, S. Ulferts, B.T. Preca, B. Hermann, J. Maurer, H. Greschik, V. Hornung, O. Einsle, S. Perner, A. Imhof, M. Jung, R. Schule, KMT9 monomethylates histone H4 lysine 12 and controls proliferation of prostate cancer cells, Nat Struct Mol Biol, 26 (2019) 361-371.

[22] C. Berlin, F. Cottard, D. Willmann, S. Urban, S.M. Tirier, L. Marx, K. Rippe, M. Schmitt, V. Petrocelli, F.R. Greten, S. Fichtner-Feigl, R. Kesselring, E. Metzger, R. Schule, KMT9 Controls Stemness and Growth of Colorectal Cancer, Cancer Res, 82 (2022) 210-220.

[23] H.M. Baumert, E. Metzger, M. Fahrner, J. George, R.K. Thomas, O. Schilling, R. Schule, Depletion of histone methyltransferase KMT9 inhibits lung cancer cell proliferation by inducing non-apoptotic cell death, Cancer Cell Int, 20 (2020) 52.

[24] S. Totonji, A. Ramos-Triguero, D. Willmann, M. Sum, S. Urban, H. Bauer, A. Rieder, S. Wang, H. Greschik, E. Metzger, R. Schule, Lysine Methyltransferase 9 (KMT9) Is an Actionable Target in Muscle-Invasive Bladder Cancer, Cancers (Basel), 16 (2024).

[25] J. Penarando, D. Willmann, M. Sum, Y. Jia, C. Berlin, L.M. Braun, Z. Chen, S. Urban, M. Jung, D. Duteil, D. Metzger, C. Gratzke, R. Zeiser, H. Greschik, R. Schule, E. Metzger, KMT9

drives T cell exclusion and dysfunction by promoting PMN-MDSCs infiltration and ARG1 expression in prostate cancer, Mol Cancer, 25 (2026).

[26] Y. Jia, S. Wang, S. Urban, J.M. Muller, M. Sum, Q. Wang, H. Bauer, U. Schulte, H. Rampelt, N. Pfanner, K.M. Schule, A. Imhof, I. Forne, C. Berlin, A. Sigle, C. Gratzke, H. Greschik, E. Metzger, R. Schule, Mitochondrial KMT9 methylates DLAT to control pyruvate dehydrogenase activity and prostate cancer growth, Nat Commun, 16 (2025) 1191.

[27] S. Wang, S.O. Klein, S. Urban, M. Staudt, N.P.F. Barthes, D. Willmann, J. Bacher, M. Sum, H. Bauer, L. Peng, G.A. Rennar, C. Gratzke, K.M. Schule, L. Zhang, O. Einsle, H. Greschik, C. MacLeod, C.G. Thomson, M. Jung, E. Metzger, R. Schule, Structure-guided design of a selective inhibitor of the methyltransferase KMT9 with cellular activity, Nat Commun, 15 (2024) 43.

[28] S. Wang, N.P.F. Barthes, S. Urban, V.I. Hazai, S.O. Klein, T. Pappert, P. Kummel, N. Heller, J. Bacher, M. Staudt, J. Ruprecht, L. Peng, M. Sum, C. Berlin, D. Sarraf, P. Regenass, R. Warstat, J. Walz, P. Mishra, L. Zhang, O. Einsle, S. Gunther, B. Breit, E. Metzger, M. Jung, R. Schule, Structure-Guided Design of a KMT9 Inhibitor Prodrug with Cellular Activity, J Med Chem, 68 (2025) 13295-13320.

[29] S. Agarwal, P.G. Hynes, H.S. Tillman, R. Lake, W.G. Abou-Kheir, L. Fang, O.M. Casey, A.H. Ameri, P.L. Martin, J.J. Yin, P.J. Iaquinta, W.R. Karthaus, H.C. Clevers, C.L. Sawyers, K. Kelly, Identification of Different Classes of Luminal Progenitor Cells within Prostate Tumors, Cell Rep, 13 (2015) 2147-2158.

[30] C.Y. Loh, J.Y. Chai, T.F. Tang, W.F. Wong, G. Sethi, M.K. Shanmugam, P.P. Chong, C.Y. Looi, The E-Cadherin and N-Cadherin Switch in Epithelial-to-Mesenchymal Transition: Signaling, Therapeutic Implications, and Challenges, Cells, 8 (2019).

[31] A. Chaves-Perez, B. Mack, D. Maetzel, H. Kremling, C. Eggert, U. Harreus, O. Gires, EpCAM regulates cell cycle progression via control of cyclin D1 expression, Oncogene, 32 (2013) 641-650.

[32] S. Chen, G. Zhu, Y. Yang, F. Wang, Y.T. Xiao, N. Zhang, X. Bian, Y. Zhu, Y. Yu, F. Liu, K. Dong, J. Mariscal, Y. Liu, F. Soares, H. Loo Yau, B. Zhang, W. Chen, C. Wang, D. Chen,

Q. Guo, Z. Yi, M. Liu, M. Fraser, D.D. De Carvalho, P.C. Boutros, D. Di Vizio, Z. Jiang, T. van der Kwast, A. Berlin, S. Wu, J. Wang, H.H. He, S. Ren, Single-cell analysis reveals transcriptomic remodellings in distinct cell types that contribute to human prostate cancer progression, Nat Cell Biol, 23 (2021) 87-98.

[33] R. Romero, T. Chu, T.J. Gonzalez Robles, P. Smith, Y. Xie, H. Kaur, S. Yoder, H. Zhao, C. Mao, W. Kang, M.V. Pulina, K.E. Lawrence, A. Gopalan, S. Zaidi, K. Yoo, J. Choi, N. Fan, O. Gerstner, W.R. Karthaus, E. DeStanchina, K.V. Ruggles, P.M.K. Westcott, R. Chaligne, D. Pe'er, C.L. Sawyers, The neuroendocrine transition in prostate cancer is dynamic and dependent on ASCL1, Nat Cancer, 5 (2024) 1641-1659.

[34] B. Baum, M. Georgiou, Dynamics of adherens junctions in epithelial establishment, maintenance, and remodeling, J Cell Biol, 192 (2011) 907-917.

[35] S. Hahn, M.O. Nam, J.H. Noh, D.H. Lee, H.W. Han, D.H. Kim, K.B. Hahm, S.P. Hong, J.H. Yoo, J. Yoo, Organoid-based epithelial to mesenchymal transition (OEMT) model: from an intestinal fibrosis perspective, Sci Rep, 7 (2017) 2435.

[36] R. Jafari, H. Almqvist, H. Axelsson, M. Ignatushchenko, T. Lundbäck, P. Nordlund, D.M. Molina, The cellular thermal shift assay for evaluating drug target interactions in cells, Nature Protocols, 9 (2014) 2100-2122.

[37] R. Jimenez-Castano, M.A. Nieto, Epithelial-to-mesenchymal transition as a central driver of tumor cell plasticity, Nat Cancer, 7 (2026) 567-582.

[38] C.X. Zhang, R.Y. Huang, G. Sheng, J.P. Thiery, Epithelial-mesenchymal transition, Cell, 188 (2025) 5436-5486.

[39] S. Yuan, R.J. Norgard, B.Z. Stanger, Cellular Plasticity in Cancer, Cancer Discov, 9 (2019) 837-851.

[40] S. Ghafoor, E. Garcia, D.J. Jay, S. Persad, Molecular Mechanisms Regulating Epithelial Mesenchymal Transition (EMT) to Promote Cancer Progression, Int J Mol Sci, 26 (2025).

[41] T.C. Brown, N.V. Sankpal, W.E. Gillanders, Functional Implications of the Dynamic Regulation of EpCAM during Epithelial-to-Mesenchymal Transition, Biomolecules, 11 (2021).

[42] N. Herranz, D. Pasini, V.M. Diaz, C. Franci, A. Gutierrez, N. Dave, M. Escriva, I. Hernandez-Munoz, L. Di Croce, K. Helin, A. Garcia de Herreros, S. Peiro, Polycomb complex 2 is required for E-cadherin repression by the Snail1 transcription factor, Mol Cell Biol, 28 (2008) 4772-4781.

[43] J. Xu, S. Lamouille, R. Derynck, TGF-beta-induced epithelial to mesenchymal transition, Cell Res, 19 (2009) 156-172.

[44] J. Yang, S.A. Mani, J.L. Donaher, S. Ramaswamy, R.A. Itzykson, C. Come, P. Savagner, I. Gitelman, A. Richardson, R.A. Weinberg, Twist, a master regulator of morphogenesis, plays an essential role in tumor metastasis, Cell, 117 (2004) 927-939.

[45] U. Burk, J. Schubert, U. Wellner, O. Schmalhofer, E. Vincan, S. Spaderna, T. Brabletz, A reciprocal repression between ZEB1 and members of the miR-200 family promotes EMT and invasion in cancer cells, EMBO Rep, 9 (2008) 582-589.

[46] B. Langmead, C. Trapnell, M. Pop, S.L. Salzberg, Ultrafast and memory-efficient alignment of short DNA sequences to the human genome, Genome Biol, 10 (2009) R25.

[47] K.P. O'Rourke, L.E. Dow, S.W. Lowe, Immunofluorescent Staining of Mouse Intestinal Stem Cells, Bio Protoc, 6 (2016).

Figure Legends

Fig 1. KMT9 promotes EMT and tumour plasticity in mouse prostate Pten/Trp53 KO tumour cells. A, Tumour mesenchymal cells (EpCAM$^-$/E-cadherin$^-$/KR5$^-$/SMA$^-$) distribution in PINs (asterisk) and invasive areas (white arrows) in WT, *Pten/Trp53* KO, and *Pten/Trp53/Kmt9*α KO prostates unravelled by single-cell phenotyping. Cell types and antibodies used for staining are indicated. Scale bars represent 50 µm. **B,** Bar graphs representing distribution and percentages of tumour mesenchymal cells in WT, *Pten/Trp53* KO PIN and invasion areas, and *Pten/Trp53/Kmt9*α KO prostates identified by single-cell spatial phenotyping (n=8). **C**, Dot blot showing expression levels of *Epcam*, *Cdh1*, *Ccnd1* and *Kmt9*α in mouse EpCam^{low} and EpCam^{high} prostate luminal epithelial cells in *Pten/Trp53* KO and

Pten/Trp53/Kmt9α KO prostates tumours. **D**, Single-cell distribution of prostate luminal EpCAM$^+$ and EpCAM$^-$ with presence (KMT9α$^+$) or absence (KMT9α$^-$) of nuclear KMT9α in WT, *Pten/Trp53* KO, and *Pten/Trp53/Kmt9α* KO prostates. Cell types and antibodies used for staining are indicated. Scale bars represent 20 µm. **E**, Bar graphs representing the percentages of EpCAM$^+$ and EpCAM$^-$ cells identified by single-cell spatial immunophenotyping in WT, *Pten/Trp53* KO, and *Pten/Trp53/Kmt9α* KO prostates (n=10). **F**, Bar graphs representing the percentage of EpCAM$^-$ cells positive (nuclear KMT9α$^+$) and negative (KMT9α$^-$) for nuclear KMT9α identified by single-cell spatial immunophenotyping in *Pten/Trp53/Kmt9α* KO prostates (n=10). **G**,**H**, Bar graphs representing the percentage of EpCAM$^-$ cells identified by flow cytometry in cultures of WT, *Pten/Trp53* KO, *Pten/Trp53/Kmt9α* KO mouse prostate luminal cells (n=5) (**G**) and in *Pten/Trp53/Kmt9α* KO compared to *Pten/Trp53/Kmt9α* KO/NLS-KMT9α mouse prostate luminal cells (n=4) (**H**). **I**, Representative flow cytometry plot with percentages of EpCAM$^+$ and EpCAM$^-$ populations in Pten/Trp53 KO cells cultures obtained before cell sorting. **J**, Representative flow cytometry plots with percentages of EpCAM$^+$ and EpCAM$^-$ populations in Pten/Trp53 KO cells cultures obtained by cell sorting 8 days after starting cultures with either a sorted population of EpCAM$^+$ (left plot) or EpCAM$^-$ (right plot) Pten/Trp53 KO cells.

Fig. 2: KMT9 controls the expression of key genes for epithelial identity. A, Western blot analysis of cytoplasmic, nuclear, and chromatin-bound fractions of lysates of unsorted, EpCAM$^+$, and EpCAM$^-$ *Pten/Trp53* KO prostate luminal cells using the indicated antibodies. Tubulinα, Lamin B1, and Histone H4 served as controls. **B**, Venn diagram showing the overlap of the number of genes differentially expressed between EpCAM$^+$ and EpCAM$^-$ *Pten/Trp53* KO prostate luminal cells and genes with presence of KMT9α at the promoter in *Pten/Trp53* KO prostate luminal cells. **C**, Enriched pathway analysis for 760 DEGs between *Pten/Trp53* KO EpCAM$^+$ and EpCAM$^-$ prostate luminal cells and genes with presence of KMT9α at the promoter. Bars represent individual Benjamini logP values derived from GO enrichment

analysis. **D**, Heatmap displaying mRNA levels of differentially expressed genes between EpCAM$^+$ and EpCAM$^-$ *Pten/Trp53* KO prostate luminal cells. Key epithelial "gate-keepers" genes such as *Epcam*, *Cdh1*, *Krt5, Krt6a, Krt14* and *Krt16* are labelled with red colour. **E**, RNA-seq tracks representing expression at representative genes in *Pten/Trp53* KO EpCAM$^+$ and EpCAM$^-$ cells and ChIP-seq tracks showing KMT9α at representative genes in *Pten/Trp53* KO mouse prostate tumour cells. **F**, RT-qPCR analysis showing relative mRNA levels of representative genes in *Pten/Trp53* KO EpCAM$^+$ and EpCAM$^-$ cells (n=3). Data represent means +s.d. **G**, Analysis of protein expression of the indicated proteins by Western blot performed in WT, *Pten/Trp53* KO *Pten/Trp53* KO EpCAM$^+$ and *Pten/Trp53* KO EpCAM$^-$ mouse prostate cells. **H**, RT-qPCR analysis showing relative mRNA levels of representative genes in WT, *Pten/Trp53* KO, *Pten/Trp53/Kmt9α* KO, and *Pten/Trp53/Kmt9α* KO/NLS-KMT9α cells (n≥3). Data represent means +s.d. Analysis of protein expression of the indicated proteins by Western blot performed in (**I**) WT, *Pten/Trp53* KO, *Pten/Trp53/Kmt9α* KO KMT9α, *Pten/Trp53/Kmt9α* KO/NLS-KMT9α mouse prostate cells, and (**J**) *Pten/Trp53/Kmt9α* KO/NLS-KMT9α, *Pten/Trp53/Kmt9α* KO/NLS-KMT9α EpCAM$^+$ and *Pten/Trp53/Kmt9α* KO/NLS-KMT9α EpCAM$^-$ mouse prostate cells using the indicated antibodies.

Fig. 3: KMT9 drives the generation of invasive mesenchymal tumour cells in *Pten/Trp53* KO tumour cells. A, Bright field and immunofluorescence staining images of *Pten/Trp53* KO unsorted, EpCAM$^+$ and EpCAM$^-$ organoids. Front-rear polarity of EMT cells is indicated with white arrows. Immunofluorescence staining was performed with the indicated antibodies. Scale bars: 100 μm. **B**, Bright field representative images of invasive cells (red arrows) in organoid cultures of *Pten/Trp53* KO unsorted, EpCAM$^+$ and EpCAM$^-$ cells. The red dashed line demarcate Matrigel border. Scale bars: 100 μm. **C**, **D**, **E**, Representative images (**C**) and graphs depicting invasion (**D**) and spheroid size (**E**) of unsorted, EpCAM$^+$, and EpCam$^-$ *Pten/Trp53* KO cells over a period of time of 10 days. Data represent means ±s.d. (n=9). Red arrows indicate presence of invasive *Pten/Trp53* KO EpCam$^-$ cells. Scale bars: 500 μm. **F**, **G**, **H**, Representative images (**F**) and graphs depicting invasion (**G**) and spheroid size (**H**) of

unsorted, EpCAM$^+$, and EpCam$^-$ *Pten/Trp53/Kmt9*α KO/NLS-KMT9α cells over a period of time of 10 days. Data represent means ±s.d. (n=4). Red arrows indicate presence of invasive *Pten/Trp53/Kmt9*α KO/NLS-KMT9α EpCam$^-$ cells. Scale bars: 1000 μm.

Fig. 4: Inhibition of KMT9 impairs EMT and blocks invasion of prostate Pten/Trp53 KO tumour mesenchymal cells. **A**, **B**, CETSA for KMT9 in *Pten/Trp53* KO cells treated with vehicle (DMSO) or 500 nM KMI169. Representative Western blots (**A**) and quantification (**B**) showing increased melting temperatures (ΔT_m) of endogenous KMT9 upon treatment with KMI169 compared to DMSO. **C**, **D**, Bar graph (**C**) and representative flow cytometry plot (**D**) showing percentages of EpCAM$^+$ and EpCAM$^-$ mouse prostate luminal cell populations in *Pten/Trp53* KO cultured in presence of vehicle and KMI169 (500 nM) for 7, 11, or 18 days. Data represent means +s.d. (n≥3). **E**, RT-qPCR analysis showing relative mRNA levels of the indicated genes in *Pten/Trp53* KO cells cultured in the presence of DMSO or 500 nM KMI169 for 72 hours. Data represent means +s.d. (n=3). **F**, **G**, **H**, Representative images (**F**) and graphs depicting invasion (**G**) and spheroid size (**H**) of *Pten/Trp53* KO EpCam$^-$ cells cultured in presence of vehicle or KMI169 (500 nM) over a period of time of 10 days. Data represent means ±s.d. (n=9). Red arrows indicate presence of invasive *Pten/Trp53* KO EpCam$^-$ cells. Scale bars: 500 μm. **I**, Loss of Pten and Trp53 genes results in the generation of a subpopulation of highly invasive mesenchymal tumour cells with lack of EpCAM expression and where chromatin occupancy of KMT9 is enhanced, resulting in the downregulation of key genes for epithelial identity, including EpCAM, Cdh1 and multiple cytokeratins. Targeting KMT9 with KMI169 impairs the generation of these mesenchymal tumour cells and blocks their invasive capacities.

Supplementary Figure 1: KMT9 promotes EMT and tumour plasticity in mouse prostate Pten/Trp53 KO tumour cells. A, UMAP plot showing the different cell populations identified by scRNA-seq in *Pten/Trp53* KO, and *Pten/Trp53/Kmt9*α KO mice prostates. **B**, **C**, Dot blot showing expression levels of *Epcam*, *Cdh1*, *Ccnd1* (**B**) and *Kmt9*α (**C**) in EpCam^{low} and

EpCam^{high} prostate luminal epithelial cells in human prostates tumours. **D**, Analysis of protein expression of the indicated proteins by Western blot was performed in WT, *Pten/Trp53* KO, *Pten/Trp53/Kmt9α* KO, and *Pten/Trp53/Kmt9α* KO/NLS-KMT9α mouse prostate luminal cells using the indicated antibodies. **E**, Representative flow cytometry plots of Lin$^-$ EpCAM$^+$ and EpCAM$^-$ WT, *Pten/Trp53* KO and *Pten/Trp53/Kmt9α* KO mouse prostate luminal cells. **F**, **G**, **H**, Representative flow cytometry plots showing percentages of EpCAM$^+$ and EpCAM$^-$ mouse prostate luminal cell populations in (**F**) *Pten/Trp53* KO (also called PtP), (**G**) *Pten/Trp53/Kmt9α* KO, *Pten/Trp53/Kmt9α* KO/NLS-KMT9α and (**H**) *Pten/Trp53/Kmt9α* KO/MTS-KMT9α. **I**, Representative images showing the different morphologies of *Pten/Trp53* KO EpCAM$^+$ and EpCAM$^-$ mouse prostate luminal cell populations 1 and 8 days after cell sorting.

Supplementary Figure 2: KM9 controls the expression of key genes for epithelial identity. A, RT-qPCR analysis showing relative mRNA levels of Ctnnb1 in *Pten/Trp53* KO EpCAM$^+$ and EpCAM$^-$ cells (n=3). Data represent means +s.d. **B**, Analysis of protein expression of the indicated proteins by Western blot was performed in WT, *Pten/Trp53* KO, *Pten/Trp53* KO EpCAM$^+$, *Pten/Trp53* KO EpCAM$^-$, and *Pten/Trp53/Kmt9α* KO mouse prostate luminal cells using the indicated antibodies. **C**, QRT-PCR analysis showing relative mRNA levels of *Ccnd1* in WT, *Pten/Trp53* KO, *Pten/Trp53/Kmt9α* KO, and *Pten/Trp53/Kmt9α* KO/NLS-KMT9α cells (n=4). Data represent means +s.d. **D**, **E**, Analysis of protein expression of the indicated proteins by Western blot was performed in WT (**D**, **E**), *Pten/Trp53* KO (**D**), *Pten/Trp53* KO EpCAM$^+$ (**D**), *Pten/Trp53* KO EpCAM$^-$ (**D**), *Pten/Trp53/Kmt9α* KO (**D**), *Pten/Trp53/Kmt9α* KO/NLS-KMT9α (**E**), *Pten/Trp53/Kmt9α* KO/NLS-KMT9α EpCAM$^+$ (**E**), *Pten/Trp53/Kmt9α* KO/NLS-KMT9α EpCAM$^-$ (**E**) mouse prostate luminal cells using the corresponding antibodies.

Supplementary Figure 3: KMT9 drives the generation of invasive mesenchymal tumour cells in *Pten/Trp53* KO tumours. A, **B**, Representative images (**A**) and graphs depicting tumour cell dissemination (**B**) of *Pten/Trp53* KO EpCam$^-$ of *Pten/Trp53* KO unsorted, EpCAM$^+$,

and EpCam$^-$ spheroids over a period of time of 3 days. Data represent means ±s.d. (n=3). Red arrows indicate presence of EMT migrating cells.

Supplementary video 1. Tumour cell Invasion of *Pten/Trp53* KO unsorted spheroids.

Supplementary video 2. Tumour cell Invasion of *Pten/Trp53* KO EpCAM$^+$ spheroids.

Supplementary video 3. Tumour cell Invasion of *Pten/Trp53* KO EpCam$^-$ spheroids.

Figure 1. KMT9 promotes EMT and tumour plasticity in mouse prostate Pten/Trp53 KO tumour cells

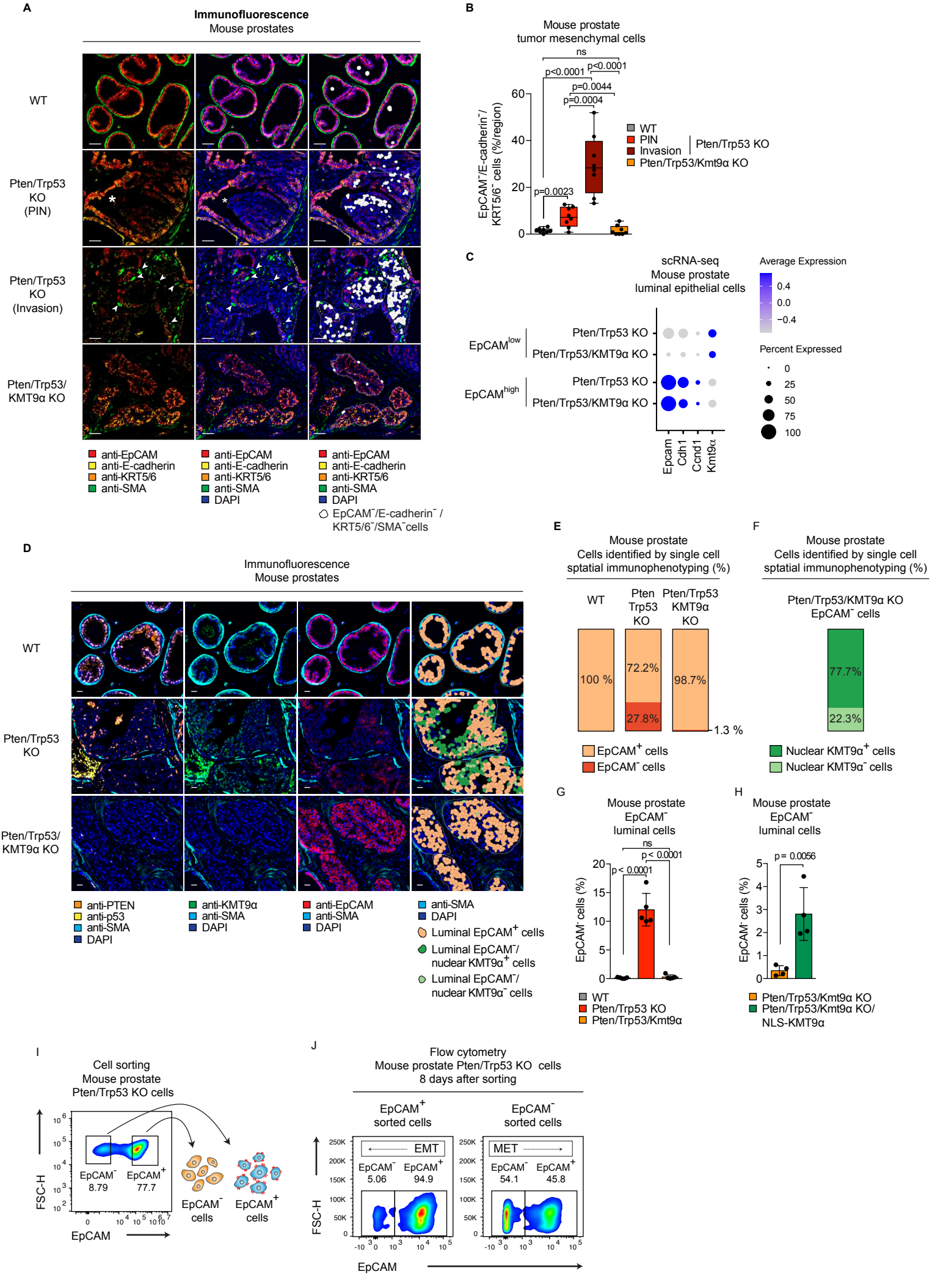

Figure 2. KMT9 controls the expression of key genes for epithelial identity

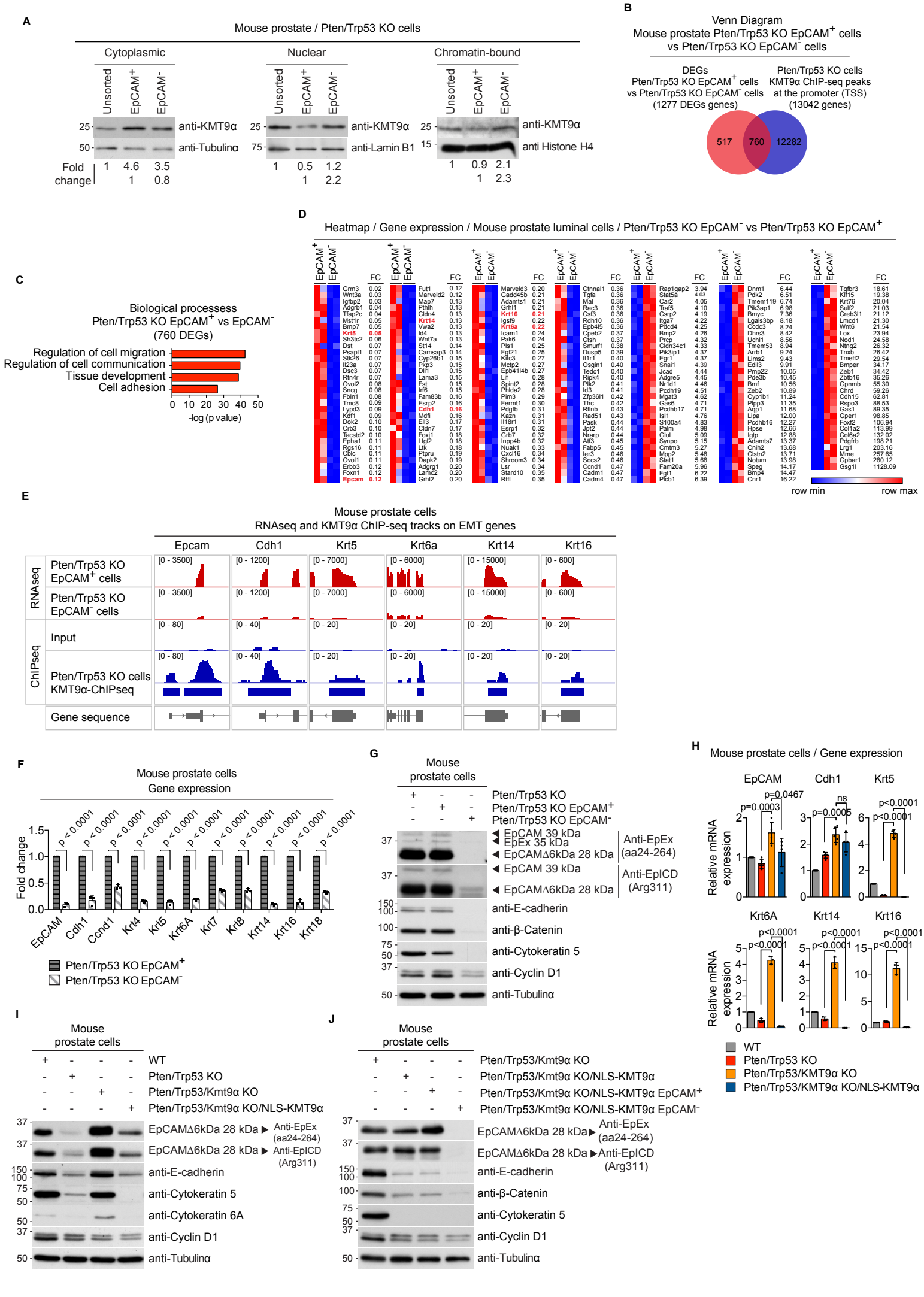

Figure 3. KMT9 drives the generation of invasive Pten/Trp53 KO mesenchymal tumour cells

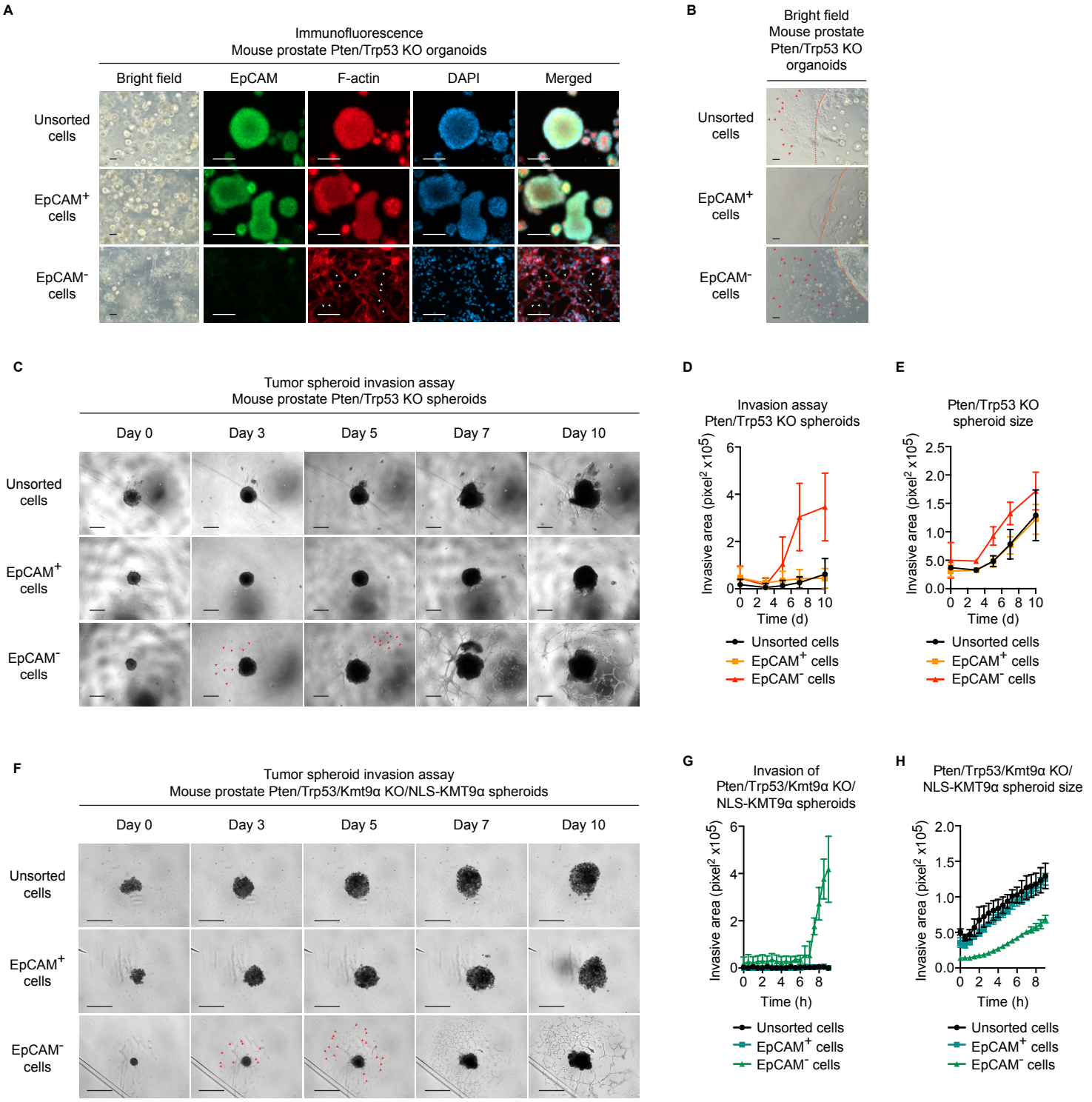

Figure 4. Inhibition of KMT9 impairs EMT and blocks invasion of prostate Pten/Trp53 KO tumour mesenchymal cells

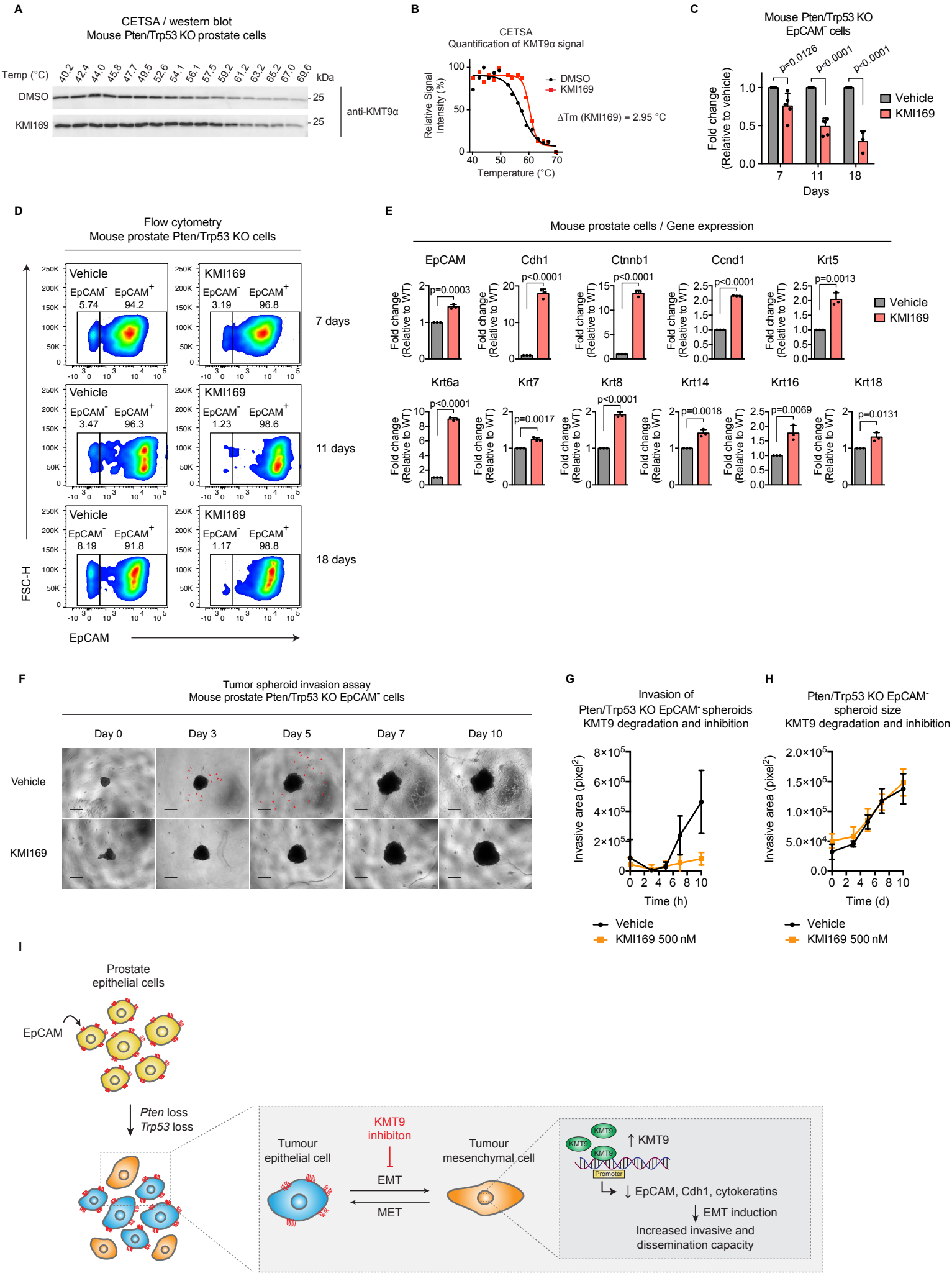

Supplementary Files

This is a list of supplementary files associated with this preprint. Click to download.

- SFigure3.pdf
- Supplementaryvideo3.mp4
- Table1.Opalpanels.xlsx
- Supplementaryvideo1.mp4
- SFigure1.pdf
- Supplementaryvideo2.mp4
- SFigure2.pdf